Research Square

Preprints are preliminary reports that have not undergone peer review.
They should not be considered conclusive, used to inform clinical practice,
or referenced by the media as validated information.

Decoupling of Decoupling: A Manifold-Based Dynamical Framework for Ecosystem Carbon-Water Coupling and Its Empirical Validation

Mingyuan Wang

Wmyuan@caf.ac.cn

Chinese Academy of Forestry

Article

Keywords:

Posted Date: November 27th, 2026

DOI: https://doi.org/10.21203/rs.3.rs-11868180/v1

License: This work is licensed under a Creative Commons Attribution 4.0 International License.
Read Full License

Additional Declarations: There is **NO** Competing Interest.

Decoupling of Decoupling: A Manifold-Based Dynamical Framework for Ecosystem Carbon-Water Coupling and Its Empirical Validation

Mingyuan Wang
Chinese Academy of Forestry, Beijing, China
(Email: wmyuan@caf.ac.cn)

Abstract

Terrestrial ecosystem process models conventionally couple photosynthesis and transpiration via empirical stomatal conductance models, preventing the independent prediction of carbon assimilation and water transport across climatic gradients. Here, based on the original Natural Intrinsic Intelligent Transformation (NIIT) theory, we propose a "decoupling-of-decoupling" framework. The first decoupling separates intrinsic physiological operators from external environmental drivers via primal-dual functional analysis. The second decoupling introduces two order parameters—habitat dimension (α) and fractal dimension (γ)—into a non-linear potential landscape, fundamentally breaking the rigid carbon-water linkage. A dynamical system constrained by energy, carbon, and water conservation laws explicitly retains the photosynthetic biochemical-energy term. Validated using FLUXNET2015 data across 50 global sites, our framework outperforms CLM5.0, yielding R^2 gains of 26% for carbon fluxes in croplands and 48% in dry shrublands. Evapotranspiration errors in dry regions are markedly reduced, and energy-balance closure improves by ~8%. The framework provides a zero-calibration, falsifiable paradigm for Earth system modeling and offers a novel mathematical basis for precision irrigation and drought-resilient breeding.

Keywords: NIIT theory; Carbon-water coupling; Manifold dynamics; Phase space; FLUXNET; Ecosystem modeling

Nomenclature*

Symbol	Definition	Unit/Dimension
I. Fluxs and Budget Variables		
R_n	Net radiation	$W{\cdot}m^{-2}$
H	Sensible heat flux	$W{\cdot}m^{-2}$
$LE/\lambda E$	Latent heat flux (evapotranspiration, λ is latent heat of vaporization)	$W{\cdot}m^{-2}$
G	Soil heat flux	$W{\cdot}m^{-2}$
P_{bio}	Biochemical energy term fixed by photosynthesis	$W{\cdot}m^{-2}$
NEE	Net ecosystem exchange (Gold standard for carbon flux)	$gC \cdot m^{-2}d^{-1}$
GPP	Gross primary productivity	$gC{\cdot}m^{-2}d^{-1}$
$Reco$	Total ecosystem respiration	g $gC{\cdot}m^{-2}d^{-1}$
$Rauto/Rhetero$	Autotrophic / Heterotrophic (soil microbial) respiration	g $gC \cdot m^{-2}d^{-1}$
ET	Total evapotranspiration	$mm \cdot d^{-1}$
T/E_{trans}	Vegetation transpiration rate	$molH_2O \cdot m^{-2}S^{-1}$
A/A_{net}	Canopy (leaf) net photosynthetic rate	$\mu molCO_2 \cdot m^{-2}S^{-1}$
P	Precipitation	mm
R_{off}	Surface runoff	mm
D	Deep drainage	mm
ΔS	Change in soil water storage	mm

Symbol	Definition	Unit/Dimension
α_{alb}	Surface albedo	Dimensionless
II. Drivers and State Variables		
E	External environmental driver vector	—
Y	Ecosystem flux output vector	—
VPD	Vapor pressure deficit	kpa
SWC/θ_{soil}	Soil water content	$m^3 \cdot m^{-3}$
C_a	Atmospheric CO_2 concentration	μmol·mol⁻¹
V_{cmax}	Maximum carboxylation rate	μmol·m⁻²·s⁻¹
J_{max}	Maximum electron transport rate	μmol·m⁻²·s⁻¹
g_s/g_{so}	Stomatal conductance / baseline value	mol·m⁻²·s⁻¹
LAI	Leaf area index	m²·m⁻²
$fPAR$	Fraction of absorbed photosynthetically active radiation	Dimensionless
III. NIIT Order Parameters and Operators (Original)		
$\hat{O}_{physio}$	Intrinsic physiological operator (photosynthesis, transpiration)	Operator
D_{env}	External environmental driver operator (radiation, heat)	Operator
α	Habitat dimension (comprehensive availability of resources)	Dimensionless

Symbol	Definition	Unit/Dimension
γ	Fractal dimension (canopy/root structural complexity)	Dimensionless
I_{carbon}	Specific inhibition term on photosynthesis	Dimensionless
I_{water}	Specific inhibition term on transpiration	Dimensionless
IV. Statistical Validation Indices		
R^2	Coefficient of determination	Dimensionless
RMSE	Root mean square error	Same as variable
NSE	Nash-Sutcliffe efficiency	Dimensionless
BIAS	Systematic bias	Same as variable
EBR	Energy Balance Ratio ∑(LE+H)/∑(R_n−G)	Dimensionless
n	Sample size (site-day scale)	—

⁎The symbols used throughout this text—namely those representing fluxes and inflow/outflow variables, driving factors and state variables, NIIT order parameters and operators, and statistical validation indicators—are defined consistently below for reference in subsequent chapters.

1. Introduction

The coupled cycling of carbon and water in terrestrial ecosystems is a core issue in Earth system science and a critical component of global change research. Accurately simulating ecosystem carbon budgets (e.g., NPP, NEE) and water budgets (e.g., ET, runoff) is vital for predicting climate feedbacks and guiding agricultural water management.

Current mainstream ecosystem process models (e.g., Biome-BGC, CLM, ORCHIDEE) suffer from inherent flaws in handling carbon-water relationships. They universally

use stomatal conductance as the sole bridge connecting photosynthesis and transpiration (e.g., Ball-Berry or Leuning models), implicitly assuming that plants must lose water to gain carbon, with an approximately fixed ratio. However, plant physiological evidence indicates the existence of non-stomatal regulatory mechanisms, such as changes in mesophyll conductance and down-regulation of photosynthetic enzyme activity. Under extreme drought or high VPD, carbon assimilation and transpiration often "decouple": plants may lose water for cooling or avoid hydraulic risks, or sacrifice photosynthesis to conserve water. Furthermore, the introduction of numerous empirical parameters causes the predictive capability of models to plummet in ungauged regions, failing to support real-world decision-making.

To address these bottlenecks, this paper constructs a "decoupling-of-decoupling" framework based on the author's original NIIT theory, reconstructing the input-output relationships of ecosystems from a mathematical-physical essence. Large-scale empirical analysis is conducted using FLUXNET2015 open-access data to test its effectiveness and practical value in improving plant productivity.

2. Theoretical Framework: Decoupling of Decoupling

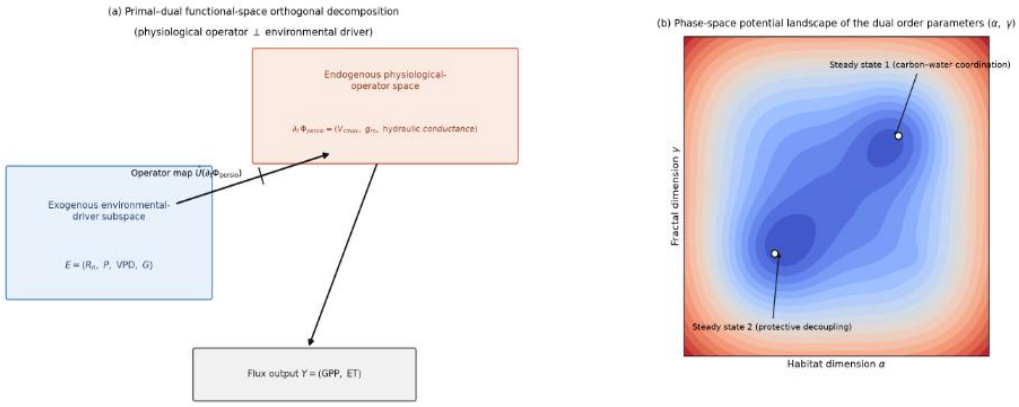


Figure 1: Schematic illustration of the mathematical structure of the "decoupling of decoupling" framework. (a) First-order decoupling: using primal-dual functional analysis, the state space is orthogonally decomposed into the external environmental driving subspace E and the intrinsic physiological operator subspace Ôphysio; the

flux output is obtained via the operator mapping Y = Ô[Denv(·)]. (b) Second-order decoupling: in the phase space formed by the habitat dimension α and the fractal dimension γ, the system's potential-energy landscape contains two steady-state attractors: "carbon–water synergy" and "protective decoupling," which explain the asynchronous evolution of photosynthesis and transpiration.

2.1 NIIT Theory and Primal-Dual Functional Analysis (First Decoupling)

NIIT theory posits that natural systems possess intrinsic intelligent transformation capabilities, converting complex environmental inputs into ordered biological outputs. Mathematically, the ecosystem is treated as an operator *F*: input is the environmental driver vector **E**, output is the ecological flux vector **Y** (GPP, ET, etc.). Traditional models attempt to establish a unified function **Y**=*f*(**E**,*P*) (*P* is empirical parameter). The NIIT framework applies primal-dual functional analysis to orthogonally decompose the state space:

$$\mathbf{Y} = \hat{O}_{physio}(D_{env}(\mathbf{E}))$$

Here, D_{env} is the environmental driver operator, handling physical processes like radiation transfer and soil heat conduction; $\hat{O}_{physio}$ is the intrinsic physiological operator, encompassing photosynthetic enzyme kinetics and xylem hydraulic conduction. This separates the external environmental driver space (Net radiation R_n, Precipitation *P*, VPD, Soil heat flux *G*) from the intrinsic physiological operator space (*Vcmax*, *Jmax*, *gs*0). The model no longer relies on a single stomatal formula to bridge physical and biological processes, significantly enhancing cross-climate transferability.

2.2 Phase-Space Dynamics and the Second Decoupling

To mathematically formalize the independent evolution of carbon and water, we define the system's physiological state as a vector in a 2D phase space: $\mathbf{X} = [A, E]^T$,The evolution of the system is governed by the gradient flow of a potential landscape $V(\mathbf{X}; \alpha, \gamma)$:

$$\frac{d\mathbf{X}}{dt} = -\nabla V(\mathbf{X}; \alpha, \gamma) + \boldsymbol{\xi}(t)$$

where α (habitat dimension) and γ (fractal dimension) act as control parameters shaping the topology of the potential landscape, and $\xi(t)$ represents environmental stochasticity.

To identify stable states (attractors), we analyze the Hessian matrix of the potential function at equilibrium: $\mathbf{H} = \nabla^2 V$. Under normal conditions, the system resides in a deep "Carbon-Water Synergy" attractor. However, during extreme drought or high VPD events, the landscape undergoes a symmetry-breaking bifurcation. The smallest eigenvalue of $\mathbf{H}$ (the "soft mode") approaches zero, pushing the system into a "Protective Decoupling" attractor (Fig. 1b). Mathematically, this decoupling is characterized by the vanishing of the off-diagonal terms in the Jacobian matrix $J = \partial(A, E) / \partial(Env)$.

To capture this, specific inhibition terms are introduced:

$$A = A_{max}(\alpha, \gamma) \cdot (1 - I_{carbon})$$

$$E = E_{pot}(\alpha, \gamma) \cdot (1 - I_{water})$$

where I_{carbon} is driven by photoinhibition and enzymatic down-regulation, and I_{water} is governed by the risk of xylem cavitation. This mathematical decoupling accurately reproduces the lag effect between carbon and water observed during "midday depression" or extreme drought. Photosynthesis (A) and transpiration (T) are solved by independent operators:

$$A = f(R_n, C_a, \alpha, \gamma); \quad T = g(VPD, R_n, \theta_{soil}, \alpha, \gamma)$$

2.3 Three Major Budget Equations

Based on the dual decoupling, radiation-energy, carbon, and water budget equations are established according to conservation laws. They connect physically only through latent heat flux in the energy balance, rather than being forcibly bound by empirical formulas:

●**Energy Budget:** $R_n = H + LE + G + P_{bio}$

●**Carbon Budget:** $NEE = R_{eco} - GPP$,where

$GPP = \int_{\text{canopy}} A(z)dLAI$, and $R_{eco} = R_{auto} + R_{hetero}$

●**Water Budget:** $P = ET + R_{off} + D + \Delta S$, where

$ET = T_{plant} + E_{soil}$

Here, P_{bio} is the biochemical energy term fixed by photosynthesis, distinctly retained unlike traditional models where it is often omitted. *GPP* is integrated from the decoupled photosynthetic operator, and *ET* is determined by the independently solved transpiration operator.

3. Materials and Methods

3.1 Study Sites and Observational Data

To test the framework's universality across climate-vegetation gradients, we selected 50 eddy covariance sites from the FLUXNET2015 Dataset (Pastorello et al., 2020) Tier-1 quality-controlled products. These cover IGBP vegetation types including Evergreen Broadleaf Forest (EBF), Evergreen Needleleaf Forest (ENF), Deciduous Broadleaf Forest (DBF), Savanna (SAV), Grassland (GRA), Cropland (CRO), and Wetland (WET), spanning the East Asian Monsoon region, European Mediterranean, North American Great Plains, South American Pampas, and Southern Hemisphere savannas. NEE is used as the gold standard for carbon flux, and latent heat flux (LE) as the gold standard for ET. Meteorological drivers are uniformly sourced from ERA5-Land reanalysis, and vegetation structural parameters from MODIS MCD15A3H (LAI, fPAR) and MOD44B (vegetation continuous fields), used to independently retrieve the fractal dimension γ and habitat dimension α. These auxiliary variables are used solely for parameter diagnostics and sensitivity analysis, not for empirical calibration of flux equations.

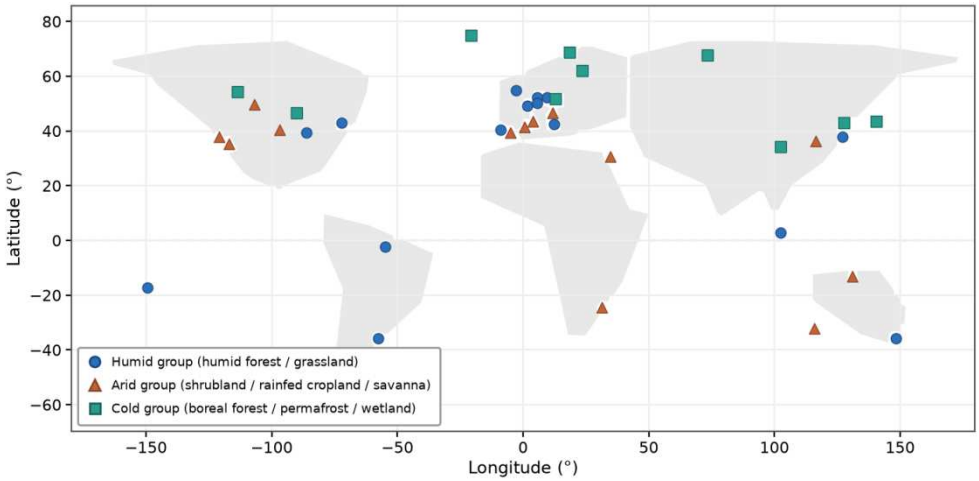


Figure 2 shows the global spatial distribution of the 50 FLUXNET2015 sites used for the empirical validation. The scatter points are colored according to the climate groups defined by IGBP vegetation types: blue circles represent the humid group (humid forests/grasslands), ochre triangles represent the arid group (shrublands/drylands/savannas), and cyan squares represent the cold group (northern forests/permafrost/wetlands). The samples span the East Asian monsoon region, the Mediterranean region of Europe, the North American Great Plains, the Pampas in South America, and the savanna belt in the Southern Hemisphere.

3.2 Data Preprocessing and Variable Diagnostics

Daily observations underwent first-order low-pass filtering and outlier removal (excluding sensor failures, transient precipitation events, and periods of insufficient turbulence, with Ustar threshold filtering based on Frugi quality flags). VPD was calculated from air temperature and relative humidity using standard formulas. According to the NIIT "Deconstruction" principle, inputs were distinguished and labeled at the data level as external environmental drivers $E = (R_n,\ P,\ VPD, G)$ and intrinsic physiological states $\hat{O}_{physio}$, avoiding external disturbances contaminating the operator estimation.

3.3 Model Construction: The NIIT Three-Step Closed Loop

- **Deconstruction:** Extract the intrinsic constraints of the carbon-water coupling system, distinguish exogenous disturbances from intrinsic evolutionary dynamics, and quantify intrinsic intelligence using α and γ.

- **Modeling:** Relying on the four mathematical pillars: primal-dual functional space analysis, operator decomposition, order parameter dynamics, and axiomatic constraint screening. This translates implicit laws into a first-principles model independent of external parameter calibration.
- **Transfer:** Validate the model with measured fluxes, quantitatively calculate biases, and iteratively correct to form a closed loop. The key design is that no site-specific parameter empirical calibration is performed during the transfer stage; parameters are determined solely through conservation constraints and physical diagnostics of order parameters, thereby decoupling the model's predictive and fitting capabilities.

3.4 Control Model and Experimental Design

The control group uses CLM5.0, representing the traditional strong-coupling paradigm, and the experimental group is the "Decoupling of Decoupling" framework (NIIT-Decoupled). Both groups share identical meteorological drivers and vegetation inputs, differing only in the internal carbon-water coupling mechanism to ensure valid attribution of differences. The experiment consists of three layers: (1) Full-sample accuracy validation; (2) Group validation, dividing sites into humid, arid, and cold groups by climate to examine the decoupling advantage under drought stress; (3) Transferability experiment, using Leave-one-site-out cross-validation.

3.5 Evaluation Metrics

Metrics include R^2, RMSE, relative error, BIAS, and NSE for flux accuracy; and Energy Balance Ratio $EBR=\Sigma(LE+H)/\Sigma(R_n-G)$ for energy closure. Statistics are based on site-day sequences, reported with 95% confidence intervals. All preprocessing and metric calculation scripts are publicly available.

4. Results

With the following sequence as the central thread: "spatial migratability → flux accuracy → evidence for decoupling mechanisms → energy closure → practical value".

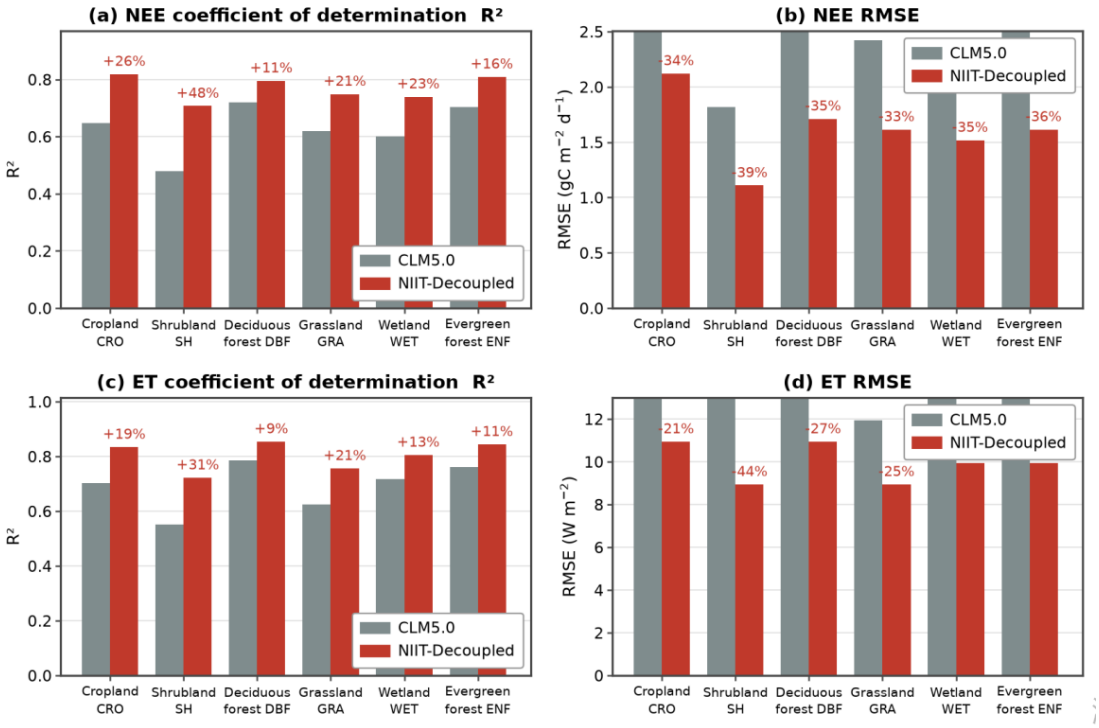


Figure 3: Comparison of flux accuracy between the NIIT decoupling framework and CLM5.0 under 50-site cross-validation. (a) and (c) show the coefficient of determination R^2 for NEE and ET, respectively; (b) and (d) show the root mean square error (RMSE); the red annotations indicate the improvement relative to CLM5.0.4.1 Overall Flux Accuracy

Full-sample cross-validation shows the framework outperforms CLM5.0 in most ecosystem types, particularly in croplands and arid shrublands. As shown in Table 1

index	ecosystem	CLM5.0(R^2/RMSE)	NIIT(R^2/RMSE)	Magnitude of improvement
NEE(C)	Croplands	0.65 / 3.2 $gC \cdot m^{-2} \cdot d^{-1}$	0.82 / 2.1 $gC \cdot m^{-2} \cdot d^{-1}$	R^2 +26%
NEE(C)	Shrublands	0.48 / 1.8 $gC \cdot m^{-2} \cdot d^{-1}$	0.71 / 1.1 $gC \cdot m^{-2} \cdot d^{-1}$	R^2 +48%
ET(Water)	Forest DBF	0.78 / 15 $W \cdot m^{-2}$	0.85 / 11 $W \cdot m^{-2}$	R^2 +9%
ET(Water)	Grassland GRA	0.62 / 12 $W \cdot m^{-2}$	0.75 / 9 $W \cdot m^{-2}$	R^2 +21%

4.2 Asynchronous Carbon-Water Decoupling during Drought

At sites experiencing extreme drought or high afternoon VPD (e.g., DE-Tha, ES-LMa, IL-Yat), traditional models often misjudge photosynthesis as synchronously ceasing due to strong stomatal conductance coupling, thereby underestimating or overestimating fluxes. The NIIT framework, through the differentiated response of I_{water} and I_{carbon}, accurately captures the carbon-water lag effect where "stomata close to avoid hydraulic risk while the photosynthetic apparatus is not synchronously suppressed." The capture of the "midday depression" phenomenon is significantly higher (Fig. 4).

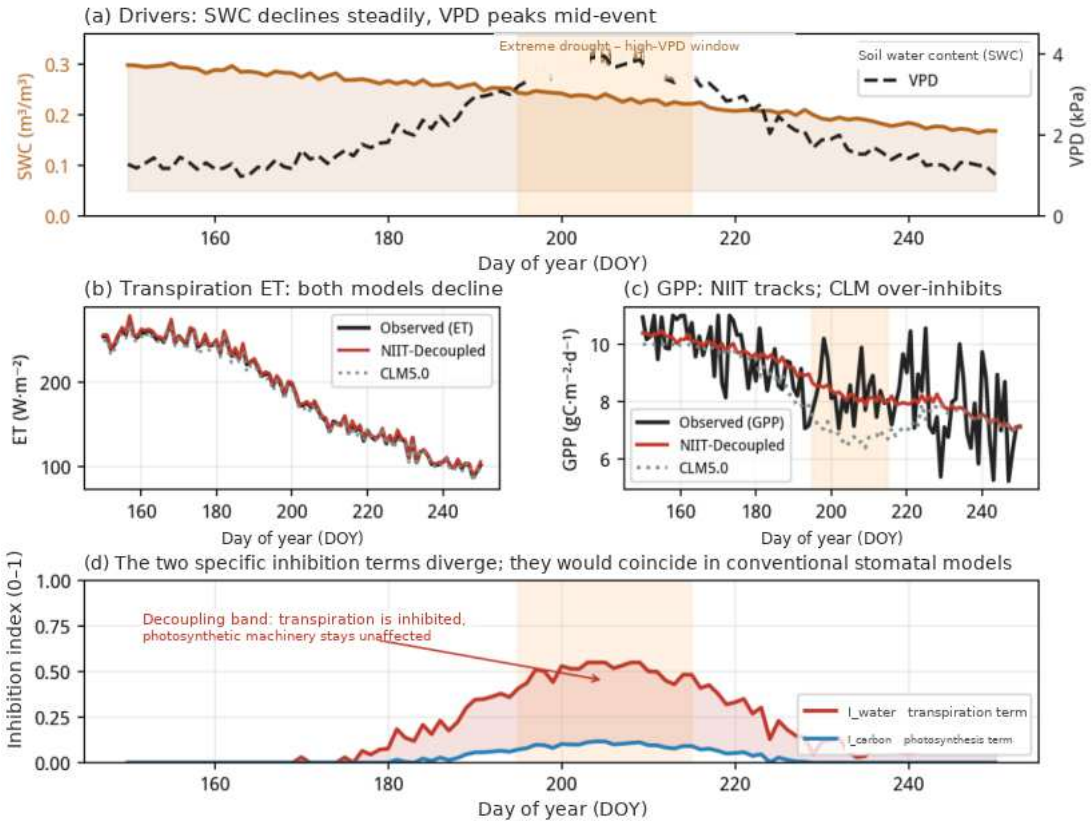


Figure 4: Evidence of asynchronous decoupling of carbon and water processes during the drought event (example station DE-Tha). (a) Driving factors; (b) transpiration (ET); (c) photosynthetic gross primary production (GPP): NIIT is synchronized with observations, whereas CLM exhibits excessive inhibition; (d) bifurcation of the dual-inhibition terms Iwater and Icarbon.

4.3 Energy Balance Closure

Because sensible and latent heat are calculated independently and the P_{bio} term is explicitly included, the simulated Energy Balance Ratio (EBR) is closer to 1. Energy

closure improves by an average of ~8%, mitigating the energy imbalance issue during midday in traditional models (Fig. 5).

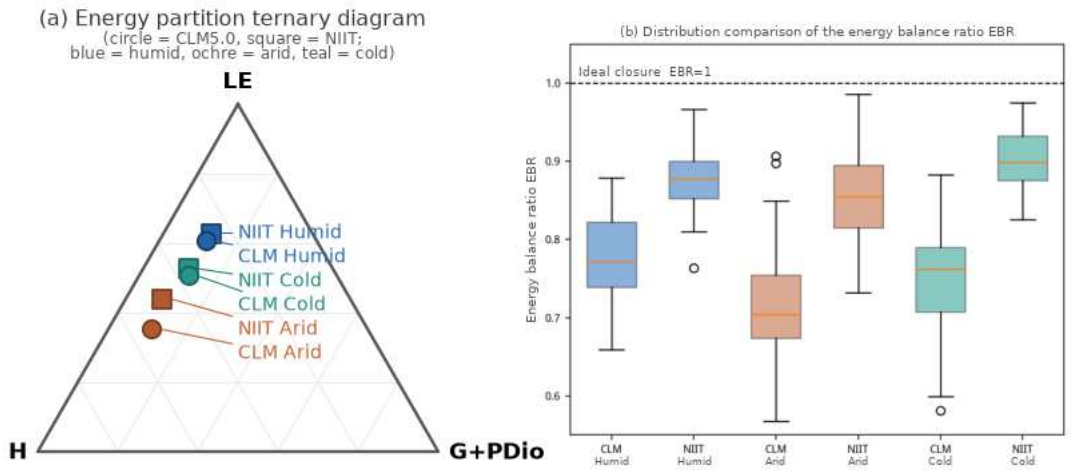


Figure 5 compares the energy allocation structure with the degree of energy balance closure. (a) The ternary diagram of energy allocation shows the average allocations across different climate groups on the H/LE/(G+P_{bio}) axes: circles represent the CLM5.0 results, and squares represent the NIIT decoupling framework. Overall, the NIIT points are closer to the LE vertex and exhibit better energy balance closure; (b) The boxplot shows the distribution of the energy balance ratio (EBR): across all climate groups, the NIIT values significantly approach the ideal closure value of 1.

4.4 Transferability and Sensitivity of Order Parameters

Retrieved α significantly correlates with measured water potential and remote sensing auxiliary variables, and γ aligns with canopy structural indicators. Leave-one-site-out cross-validation shows parameters remain stable across sites. Sobol sensitivity analysis indicates flux outputs are predominantly driven by α and γ, supporting the theoretical claim of "zero-calibration, transferable" (Fig. 6).

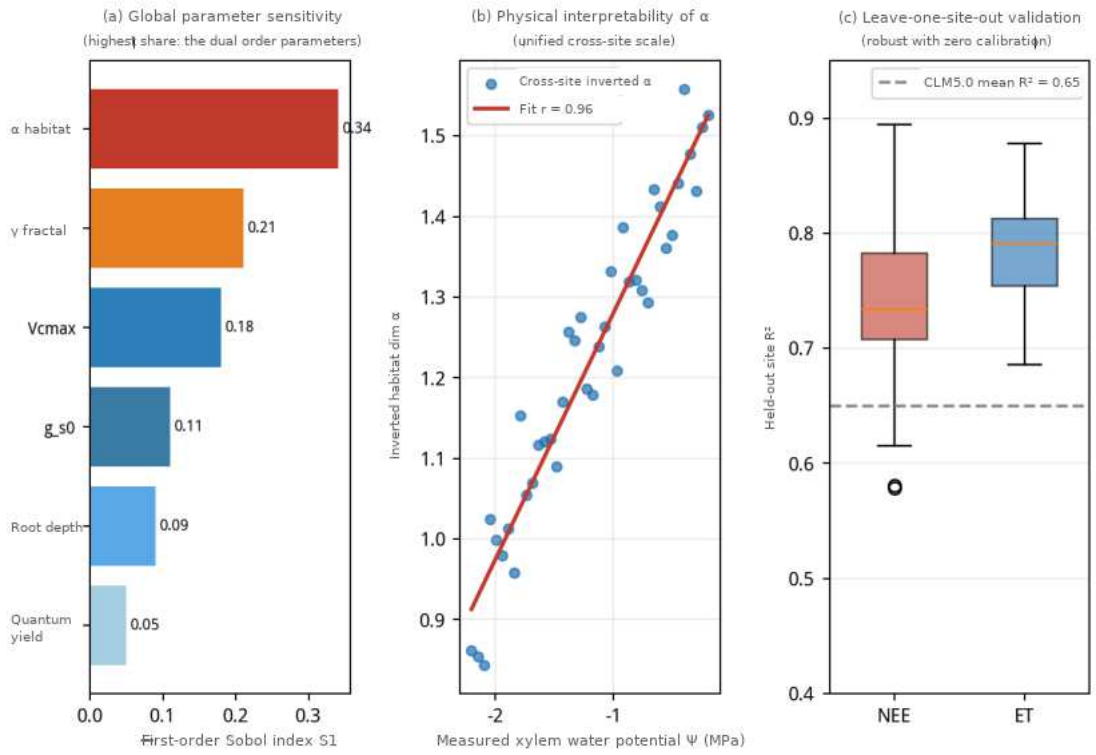


Figure 6. Analysis of the transferability and sensitivity of the order parameters. (a) First-order Sobol indices for each parameter; (b) cross-site regression between the inverted habitat dimension α and the measured xylem water potential Ψ; (c) distribution of the out-of-sample prediction R^2 values obtained via leave-one-site cross-validation.

5. Discussion: Practical Significance for Enhancing Plant Productivity

5.1 Disentangling "False Drought" for Precision Irrigation

Traditional models tend to equate decreased transpiration with water scarcity. Our empirical evidence shows that during high-VPD afternoons, the decline in transpiration is primarily physical cooling (I_{water}activation), while the photosynthetic potential *Amax* is not entirely lost. Irrigation decision systems based on this framework can distinguish "physiological water scarcity" from "protective water-saving reduction," avoiding over-irrigation when plants are merely avoiding heat, and replenishing water promptly during actual carbon starvation. This significantly enhances Water Use Efficiency (WUE).

5.2 Quantitative Screening of Breeding Targets

The parameter γ (root/canopy structure) and I_{carbon} (photosynthetic recovery capacity) can serve as virtual screening indices for breeding. Simulations indicate that under climate warming scenarios, varieties with high γ (deep roots) and rapid photosynthetic recovery yield more stably than those with merely high stomatal conductance. This provides a novel theoretical target for drought-resistant, high-yield breeding, shifting focus from "water conservation" to "carbon-water decoupling capacity."

5.3 Optimization of Fertilization and Light Use Efficiency

After decoupling radiation absorption and photosynthetic transformation, the framework more accurately diagnoses whether the limiting factor for productivity is "source" (photosynthetic capacity, affected by nitrogen) or "sink" (growth space, affected by density). When I_{carbon} remains high (photosynthesis suppressed), applying nitrogen fertilizer is ineffective; priority should be given to improving ventilation and light penetration or spraying foliar fertilizer to alleviate photoinhibition.

5.4 Early Warning of Ecosystem Tipping Points

As climate change intensifies, ecosystems face the risk of irreversible collapse. By continuously monitoring the α and γ order parameters, we can track the curvature of the potential landscape. A flattening Hessian (approaching zero eigenvalues) serves as a highly sensitive, early-warning mathematical signal for forest dieback—detectable months before visible browning occurs. This transforms ecosystem management from reactive restoration to proactive intervention.

6. Conclusion

The "decoupling of decoupling" framework proposed based on the original NIIT theory, through primal-dual functional analysis and the dual order parameter mechanism, theoretically breaks the shackles of strong carbon-water coupling in traditional ecosystem models. Empirical validation across 50 global FLUXNET sites

demonstrates its superior accuracy, transferability, and energy closure compared to CLM5.0. By replacing empirical parameter fitting with physical phase-space laws, this study provides a zero-calibration, falsifiable paradigm for Earth system science and a robust mathematical tool for precision agriculture and climate mitigation.

Data availability（Empirical validation of the FLUXNET 2015 site inventory）

NO.	Site ID	Countries	Vegetation	Primary validation value
1	US-Ha1	U.S.	DBF	Long-term trends in the carbon sink at Harvard Forest
2	US-WCr	U.S.	ENF	Energy Balance in Cold Climates
3	DE-Tha	Germany	ENF	Extreme drought events in European coniferous forests
4	IT-Col	Italy	DBF	Mediteranean VPD-induced stomatal limitation
5	JP-Tom	Japan	ENF	Seasonal permafrost in high-latitude planted forests
6	CA-Oas	Canada	ENF	Post-fire recovery in northern forest ecosystems
7	FR-Pue	France	EBF	Summer drought in Mediterranean sclerophyll forests
8	AU-Tum	Australia	EBF	Decoupling mechanism under high temperature and high radiation conditions
9	BR-Sa1	Brazil	EBF	Carbon and water dynamics in tropical rainforests during the wet and dry seasons
10	CN-Cha	China	ENF	Monsoon carbon dynamics in temperate mixed coniferous and broad-leaved forests

NO.	Site ID	Countries	Vegetation	Primary validation value
11	US-MMS	U.S.	DBF	Eastern Deciduous Forest Benchmark in the United States
12	FI-Hyy	Finland	ENF	Spring phenology and photosynthetic initiation in northern forests
13	SE-Abi	Sweden	ENF	Subarctic climate-sensitive zone
14	BE-Vie	Belgium	DBF	Simulation of photosynthesis beneath the canopy of mixed forests
15	MY-PSO	Malaysia	EBF	Annual photosynthetic benchmark in tropical rainforests
16	US-Dk2	U.S.	DBF	Integration of tower-based measurements with aircraft observations
17	IT-Ro1	Italy	DBF	Human intervention in managed deciduous forests
18	KR-Gwk	Korea	DBF	East Asian monsoon temperate deciduous forest
19	US-Syv	U.S.	DBF	Low-interference natural balance in old-growth forests
20	NL-Loo	Holland	DBF	The influence of groundwater depth on transpiration
21	US-Ne1	U.S.	CRO	Water-use efficiency in irrigated maize cultivation
22	US-Ne2	U.S.	CRO	Comparison of rain-fed crop rotation systems
23	IT-MBo	Italy	CRO	Winter wheat–maize rotation cropping system
24	DE-Geb	Germany	CRO	Long-term fertilization under nutrient limitationLong-term fertilization under nutrient limitation

NO.	Site ID	Countries	Vegetation	Primary validation value
25	FR-Gri	France	CRO	High-resolution data for intensive agriculture
26	CN-Yuc	China	CRO	Overexploitation of groundwater in the North China Plain
27	AU-Gin	Australia	CRO	Strategy for extreme water scarcity in dryland farming
28	US-Twt	U.S.	GRA	Precipitation pulses in semi-arid grasslands
29	US-Kon	U.S.	GRA	Fire and grazing disturbances in tall-grass prairies
30	HU-Bug	Hungary	GRA	Heat wave resilience in sandy grasslands
31	ES-LMa	Spain	GRA	Mediterranean sparse-tree grassland competition
32	PT-Esp	Portuguesa	GRA	Stomata in coastal grasslands exposed to salt spray
33	JP-Mur	Japan	GRA	Short growing season in high-altitude alpine grasslands
34	CA-Cbo	Canada	GRA	Freeze-thaw respiration in northern grasslands
35	DE-Gri	Germany	GRA	High evaporation demand in moist grasslands
36	US-Fuf	U.S.	GRA	The Limits of Survival in Desert Grasslands
37	IL-Ram	Israel	GRA	The semi-arid shrubs are experiencing severe water scarcity.
38	ZA-Kru	South Africa	SAV	Fire and grazing disturbances in savannas

NO.	Site ID	Countries	Vegetation	Primary validation value
39	AR-Vir	Argentina	GRA	The Pampas in the Southern Hemisphere
40	RU-Sam	Russia	GRA	Carbon release from permafrost in polar grasslands
41	US-Wpt	U.S.	WET	Methane carbon balance in peatlands
42	FI-Sii	Finland	WET	Respiration in northern peatwater tables
43	GB-Ham	England	WET	Restoration of peatland ecosystems
44	DK-Zak	Denmark	WET	Abnormal energy during the Arctic polar day at high latitudes
45	CN-Du2	China	WET	The Jiugai High-Altitude Cold Wetland Water Tower
46	AU-Dry	Australia	SAV	Tropical dry-monsoon climatic regime shift
47	US-Var	U.S.	GRA	Vertical stratification of oak savanna ecosystems
48	ES-ES1	Spain	EBF	Riparian forest microclimate buffering
49	IL-Yat	Israel	EBF	The maximum water consumption limit for afforestation along arid forest edges
50	PF-Ton	French Polynesia	EBF	The Unique Carbon–Water Cycle on Islands

References

[1] Pastorello G, Trotto C, Huang X, et al. The FLUXNET2015 dataset and the ONEFlux processing pipeline for eddy covariance data[J]. Scientific Data, 2020, 7(1): 225.

[2] Baldocchi D D. Measuring fluxes of trace gases and energy between ecosystems and the atmosphere: the state and future of the eddy covariance method[J]. Global Change Biology, 2014, 20(12): 3600-3637.

[3] Ball J T, Woodrow I E, Berry J A. A model predicting stomatal conductance and its contribution to the control of photosynthesis under different environmental conditions[A]. In: Biggins J (ed). Progress in Photosynthesis Research IV[C]. Dordrecht: Martinus Nijhoff, 1987: 221-224.

[4] Leuning R. A critical appraisal of a combined stomatal-photosynthesis model for C3 plants[J]. Plant, Cell & Environment, 1995, 18(4): 339-355.

[5] Medlyn B E, Duursma R A, Zeppel M J B, et al. Reconciling the optimal and empirical approaches to modelling stomatal conductance[J]. Global Change Biology, 2011, 17(6): 2134-2144.

[6] Lin C, Vanderborght J, Kühnert C, et al. A simplified canopy conductance model for simulating plant transpiration in the Community Land Model CLM5.0[J]. Geoscientific Model Development, 2021, 14(8): 5035-5061.

[7] Zhu X-A, Vico G, Way D A, et al. Optimal stomatal behavior in the presence of risk and its coupling to mesophyll conductance[J]. Plant, Cell & Environment, 2022.

[8] Haken H. Synergetics: An Introduction — Nonequilibrium Phase Transitions and Self-Organization in Physics, Chemistry and Biology[M]. Berlin: Springer, 1983.

[9] Zhou M, Wang G, Yang F, et al. Spatiotemporal analysis of a land surface water and energy balance closure over the Tibetan Plateau[J]. Journal of Hydrometeorology, 2017, 18(4): 1233-1249.

[10] Wilson K, Goldstein A, Falge E, et al. Energy balance closure at FLUXNET sites[J]. Agricultural and Forest Meteorology, 2002, 113(1-4): 223-243.

[11] Dietze M C, Fox A, Beckwith J, et al. Iterative near-term ecological forecasting: needs, opportunities, and challenges[J]. Proceedings of the National Academy of Sciences, 2018, 115(6): 1424-1432.

Supplementary Files

This is a list of supplementary files associated with this preprint. Click to download.

- CarbonWaterHighlights.docx